Chemical Science

Accepted Manuscript

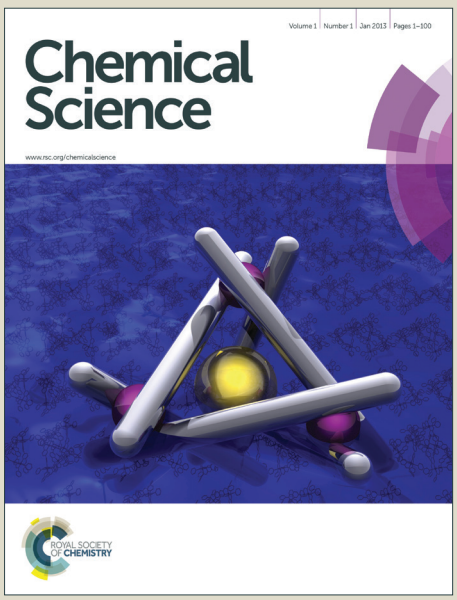

ROYAL SOCIETY OF CHEMISTRY

www.rsc.org/chemicalscience

Chemical Science

RSCPublishing

ARTICLE

NIR Electrochemiluminescence from Au_{25}^- Nanoclusters Facilitated by Highly Oxidizing and Reducing Co-reactant Radicals

Mahdi Hesari, Mark S. Workentin* and Zhifeng Ding*

Cite this: DOI: 10.1039/x0xx00000x

Received 00th January 2012,
Accepted 00th January 2012

DOI: 10.1039/x0xx00000x

www.rsc.org/

The well-defined electrochemical features and optical properties of the stable negatively charged Au_{25} clusters (Au_{25}^-) provide opportunities for a photoelectrochemical study by means of electrochemiluminescence (ECL) technique. Under annihilation conditions where the Au_{25}^- is electrochemically pumped to its various oxidized and reduced forms showed no appreciable ECL light emission, due presumably to the short lifetime of the electrogenerated intermediates. Very interestingly, in either Au_{25}^-/tri-*n*-propylamine (TPrA) or Au_{25}^-/benzoyl peroxide (BPO) co-reactant systems, the correspondingly highly reducing and oxidizing intermediates electrogenerated from TPrA and BPO lead to great light emissions at 950 and 890 nm in near-infrared (NIR) region. The ECL in the presence of various concentrations of TPrA (6.3, 12.5, 25, 50, 100 and 200 mM) and BPO (2.5, 5, 25 and 50 mM) was explicitly investigated. Along with the concentration dependence study, spooling ECL spectroscopy provided us insight into ECL mechanisms. Notably, while the Au_{25}^{-*} is the main light emission source with BPO, ECL in the presence of TPrA is attributed to emissions from the Au_{25}^{-*}, Au_{25}^{0*} and Au_{25}^{+*} that are tuneable by means of the applied potential and TPrA concentration.

Introduction

Electrochemiluminescence or electrogenerated chemiluminescnce (ECL) [1, 2] is based on light emission from an excited state formed in the course of electron transfer processes (ET) between radical cations and anions of a luminophore, electrogenerated at a working electrode. ECL can be greatly enhanced by means of reactions of luminophore radicals with highly oxidizing or reducing radicals from co-reactants such as tri-*n*-propylamine (TPrA)[3, 4] and benzoyl peroxide (BPO),[5] produced electrochemically. ECL has found a wide range of applications such as in immunoassay[6, 7] in the presence of various water soluble co-reactants.[2] There have been many reports on luminescent molecules emitting in the visible region, while near infrared (NIR) ECL emitters such as graphite oxide[8] and quantum dots are scarce.[9] NIR light at low wavelengths of the range between 700 and 2000 nm is very useful in bio-imaging techniques, which is not absorbed by cells and tissues.[10] Gold clusters (size < 2 nm) were recently introduced as ECL emitters in the *visible* range, from which the ECL signal was employed as an analytical probe for measuring organic and inorganic species.[11, 12] In contrast, we subsequently discovered that well-defined $Au_{25}(SC_2H_4Ph)_{18}^+$ (Au_{25}^+, SC_2H_4Ph = phenylethanethiol) clusters emit NIR-ECL in 1:1 acetonitrile:benzene electrolyte solution through both the annihilation and co-reactant (with BPO) routes.[13] We elucidated ECL mechanisms, where the ECL was originated from the Au_{25}^{-*} emitting in NIR region upon relaxation to its ground state. We suggest that the NIR ECL was probably from the electron transition across the highest occupied molecular orbital (HOMO) and lowest unoccupied molecular orbital (LUMO) mainly contributed from the Au_{13} core in the Au_{25}^+. The intensity of the emitted light during annihilation was found to be very weak, likely due to the very short lifetime and slow reactivity of the reactive Au_{25}^{2-}/Au_{25}^+ species generated electrochemically. Subsequently, BPO was utilized to enhance the ECL intensity. Both the Au_{25}^+ and BPO were electrochemically reduced to form the Au_{25}^{2-} and highly oxidizing benzoate radical that further reacted to generate the emissive Au_{25}^{-*}.

Herein, we report our discovery on the ECL mechanisms of the more stable $Au_{25}(SC_2H_4Ph)_{18}^-$ (abbreviate as Au_{25}^-) in the presence of both TPrA and BPO as co-reactants, from which electrogenerated radicals possessing high reducing ($E^\circ_{TPrA^\bullet}$ = -1.7 V *vs*. SCE)[3] and oxidizing ($E^\circ_{benzoate^\bullet}$ = +1.5 V *vs*. SCE)[14] power were generated, respectively. The Au_{25}^- is relatively easy to prepare and the crystal structure is known. This Au cluster is also well-established for many applications such as in catalysis.[15] Importantly, it shows rich and well-defined electrochemical and optical data that provide the necessary information allowing one to more easily understand the electronic structure, necessary for fundamental studies including ECL. Given the easily accessible redox states [Au_{25}^q (q= 2-, 1-, 0, 1+, 2+)] from this stable Au_{25}^- precursor, which can be easily electrogenerated in the vicinity of electrode, there are a number of plausible electron transfer processes between them and either the $TPrA^\bullet$ or the benzoate radical electrogenerated from the corresponding co-reactant. As a result, a wide-range of excitation states are expected to be

accessible. We will show the electrogenerated excited states emitting at 950 and 890 nm in the NIR region. The states responsible for these NIR emissions were confirmed by comparison of the ECL to the photoluminescence spectra of the *in-situ* generated three Au_{25} clusters, Au_{25}^{q} (q=1-, 0 and 1+). The ECL mechanisms/states were assigned using our spooling ECL spectroscopy, which gave insight into controlling ECL emissions in the wavelength and intensity by means of the applied potential and co-reactant concentrations. These fundamental ECL studies of Au clusters, in this case the Au_{25}, are beneficial for further understanding their electronic structures and are anticipated to lead to electroanalytical detections or bio-imaging.

Experimental

Chemicals

Tetrachloroaurate trihydrate, tetra-*n*-octylammonium bromide, tetrahydrofurane, phenylethane thiol, sodium borohydride, tri-*n*-propyl amine, benzoyl peroxide, dry acetonitrile, dry benzene, terabutylammonium perchlorate and Deuterated dichloromethane were purchased from Aldrich. Ethanol (95%) was obtained from Commercial Alcohol Inc.

Au_{25}^{-} Cluster Synthesis

$Au_{25}(SC_2H_4Ph)_{18}TOA$ (Au_{25}^{-}) was synthesized following the established protocol by Murray *et al.*[16]. Briefly 1.05 g (2.66 mmol) Au^{3+} salt and 1.66 g (1.2 eq.) were co-dissolved in 100 mL THF. The dark–red solution was cold to 0°C and then 6 eq. thiol was added to the mixture. After 2 hours, a colorless mixture was obtained, indication of –(Au-S-Au-S)- polymer formation. At this point, 10 eq. of sodium borohydride was dissolved in 20 mL MilliQ water and added to the mixture while stirring vigorously. The mixture was left to react for 5 days and then gravity filtered to separate away the side product(s). The purification consisted of washing the filtrate repeatedly with ethanol/water mixture to obtain brown solid. The pure $Au_{25}(SC_2H_4Ph)_{18}$.TOA was extracted from the solid using acetonitrile. The cluster was crystallized and then the sample purity as verified using UV-Vis-NIR (Figure S1), ^{1}HNMR (Figure S2) spectroscopy and ESI mass spectrometry (Figure S3).[13, 17]

Characterization

^{1}HNMR spectra were recorded on a Varian Mercury 400 MHz in CD_2Cl_2. The UV-vis-NIR spectroscopy was carried out using Cary 5G spectrometer in 1:1 acetonitrile: benzene mixture. Photoluminescence (PL) spectra were measured on an Acton spectrograph equipped with an Andor BR-DD CCD camera that was cooled to -65 °C prior to the experiments. An AB Applied Biosystem mass spectrometer (4700 Proteomics Analyzer) was employed to obtain the MALDI-TOF spectra. The sample was prepared by mixing a 0.2:1000 analyte: matrix ratio. Then, 7 µL of the mixture was cast on the target plate and air-dried. A MicrOTOF (Bruker) mass spectrometer was used to record ESI mass spectra of Au_{25}^{-} in CH_2Cl_2/methanol solvent mixture.

Electrochemistry, ECL and spectrophotoelectrochemistry

The electrochemical and electrochemiluminescence experiments were performed in a glass cylinder (20 cm in length and 15 mm in diameter) with a flat Pyrex window at the bottom for light detection. The above ECL cell was placed on top of a photomultiplier tube or spectrograph and camera set to record ECL-voltage curves and accumulated/spooling ECL spectra, respectively. The wavelength was calibrated prior to each experiment using a Mercury lamp.

A solution of the Au_{25}^{-} (0.1 mM) was prepared in a glovebox using dry 1:1 acetonitrile: benzene mixture. After studying the electrochemistry of the sample various concentrations of TPrA, namely 6.3, 12.5, 25, 50, 100, and 200 mM were added to the solution under Ar atmosphere. A 2 mm diameter Pt disc embedded in glass and two Pt wires served as working, reference and counter electrodes, respectively. All the potentials were calibrated against the Fc/Fc^+ redox couple with respect to the saturated calomel electrode (SCE) ($E_{Fc/Fc+}$ = 0.342 V *vs*. SCE).[18] Further details about the ECL set up can be found in ref. 13.

The PL spectra of various Au_{25} charge states were obtained by electrolysis at the appropriate potentials (*vide infra*) of a 0.1 mM Au_{25}^{-} electrolyte solution, freshly prepared under Ar atmosphere in a 1 mm thin layer quartz cell (BASi). The electrolysis was performed using a Pt mesh as the working electrode, a Ag wire immersed in 0.01 M Ag^+ / 0.1 M TBAP in acetonitrile as the nonaqueous reference electrode, and a Pt wire as the counter electrodes.[19] A 532 nm laser was utilized to irradiate the mesh electrode area, where the various charged Au_{25} species were electrochemically produced *in-situ*, while the PL signal was acquired from the narrow side of the thin layer solution by means of the same CCD camera and Acton spectrograph set. A long-pass edge filter was placed between the sample and the spectrograph entrance to cut the excitation wavelength and harmonic peaks. For instance, PL spectra of the Au_{25}^{0} and Au_{25}^{+} were obtained via *in-situ* PL acquisition of electrolyzed solution biased at 0.05 and 0.32 V *vs*. SCE, respectively.

Results and Discussion

Electrochemistry, spectroscopy and ECL in the annihilation route

Figure 1 illustrates differential pulse voltammograms (DPVs) of 0.1 mM Au_{25}^{-} clusters in 1:1 acetonitrile: benzene mixture containing 0.1 M tetra-*n*-butylammonium perchlorate (TBAP) as the supporting electrolyte. The electrochemical investigation on this cluster matched those reported by the Murray and Jin groups.[20, 21] Briefly, in the potential range between -1.90 and 1.10 V, four redox waves with formal potentials of -1.640, 0.038, 0.280 and 0.949 V *vs.* SCE can be observed, corresponding to electrochemical reactions of

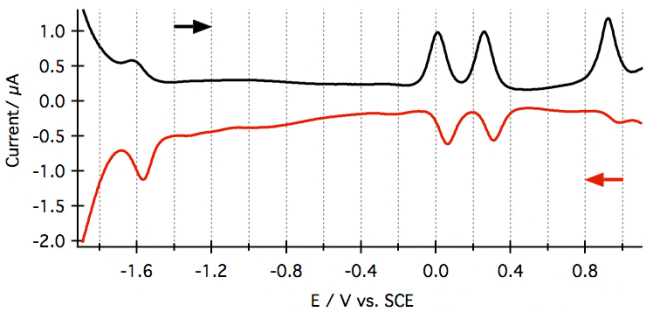

Figure 1. Differential pulse voltammotry of 0.1 mM Au_{25}^{-} in 1:1 acetonitrile: benzene containing 0.1 M TBAP. Scan rate was at 100 mVs^{-1}. Arrows in the figure show potential scan directions.

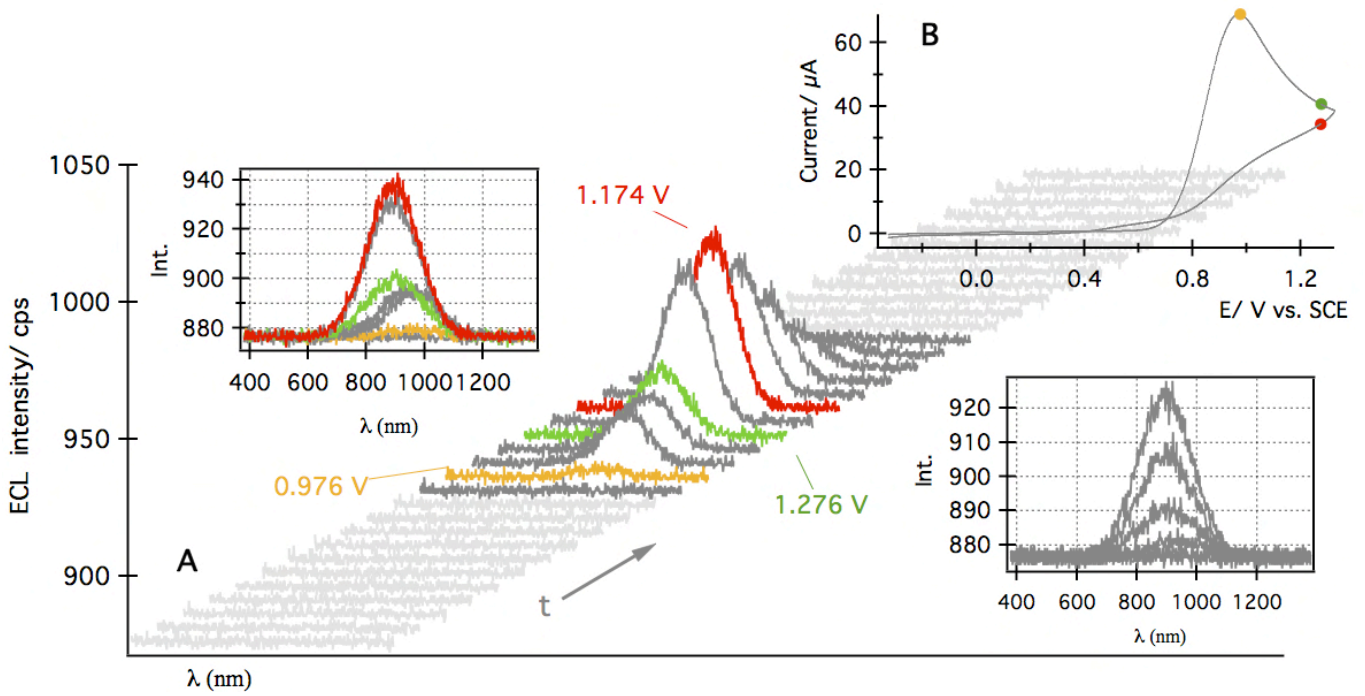

Figure 2. Spooling ECL spectra of 0.1 mM Au_{25}^- in the presence of 12.5 mM TPrA in 1:1 acetonitrile:benzene containing 0.1 M TBAP during the potential scan from -0.33 V to 1.33 V and back to -0.33 V at a scan rate of 100 mVs^{-1} (A) along with the cyclic voltammogram (B). An Andor BB-DD CCD camera (cooled at -65°C) was used to acquire the spectra at a time interval of 1 s or potential interval of 100 mV. Insets represent stack spectra of spooling for clarity of the corresponding wavelength where the same color-coded PL evolution (left inset) and devolution (left inset) are illustrated.

Au_{25}^{2-}/Au_{25}^-, Au_{25}^-/Au_{25}^0, Au_{25}^0/Au_{25}^+ and Au_{25}^+/Au_{25}^{2+} redox couples, respectively. The anodic (black) and reversed cathodic (red) potential scan demonstrate the quasi-reversible nature for the conversion between the Au_{25}^- and Au_{25}^0, and for that between the Au_{25}^0 and Au_{25}^+. The Au_{25}^{2-} and Au_{25}^{2+} are not stable as illustrate by the decreased anodic and cathodic peak heights relative to their counterparts, respectively. The HOMO-LUMO energy gap, determined from the first oxidation and reduction peak potential difference after the charge correction,[22] is 1.33 eV which is in close agreement with the reported value.[20] Similar energy gap value ca. 1.36 eV can also be calculated from the onset of UV-Vis-NIR absorption spectrum (Figure S1). The above physicochemical properties along with the crystal structure of the $Au_{25}(SC_2H_4Ph)_{18}.TOA$[23, 24] and calculated electronic structure as well as their correlations to the UV-Vis-NIR[24] and PL data,[25, 26] particularly those obtained from the PL spectra of the different charges[19] give a roadmap of photoelectrochemistry for the Au_{25}^- cluster.

ECL of the Au_{25}^- cluster was then investigated. In a typical annihilation ECL experiment, 0.1 mM Au_{25}^- in 1:1 acetonitrile: benzene electrolyte was used, where the applied potential at the working electrode was swept between -1.8 and 1.2 V vs. SCE. As depicted by the ECL-voltage curve in Figure S4, no appreciable ECL was observed. This is most likely due to the low reaction rate of the two cluster cores and the short lifetime[27] of the electrogenerated reactive intermediates Au_{25}^{2-} and Au_{25}^{2+} that did not permit a significant concentration of both species to react for any ECL generation. The low stability of the two radicals can be surmised from the irreversibility of the two reactions on the most right and left positions in the DPVs at a slow scan rate in Figure 1.

ECL of the Au_{25}^- in the presence of TPrA

Notably, the addition of a co-reactant such as TPrA could greatly enhance the ECL intensity. TPrA is suitable for our study due to the rich electrochemistry of the Au_{25}^- in the anodic region (Figure 1). TPrA undergoes an oxidative process, forms the corresponding TPrA radical cation that then deprotonates rapidly to generate the highly reducing TPrA$^\bullet$ (E°= -1.7 V *vs.* SCE) (eqs. 1-2).[3] This provides an appropriately high concentration of a highly reducing species in solution to react with the short-lived oxidized form of the Au_{25}^-. To this end, various TPrA concentrations, ranging from 6.3, 12.5, 25, 50, 100, to 200 mM were added for the ECL enhancement in the 0.1 mM Au_{25}^- solution. Figure 2 demonstrates the results from a typical experiment where 12.5 mM TPrA was added to a 0.1 mM solution of the Au_{25}^-. Panel A in Figure 2 shows the spooling ECL spectra as a function of the applied potential. This technique, that we have coined as spooling ECL spectroscopy, allows one to track the changes in the ECL emission peak wavelength and intensity with the corresponding potential. The spooling spectra were obtained within 66 seconds, with an interval of 1 s in the course of 2 cycles of potential scanned from -0.327 V to 1.325 V and back to -0.327 V, at a scan rate of 100 mVs^{-1}. The corresponding cyclic voltammogram, which is dominated by the oxidation of relatively high concentration of TPrA, is shown in panel B. The color-coding represents correlations of the spooling ECL spectra to the potential on the CV. Additional details about ECL spectral peak positions can be clearly seen when the spectra are plotted as stacked spectra (insets) showing ECL intensity evolution (left inset) and devolution (right inset) with the potential change.

The onset emission was observed at a potential of 0.976 V, with a peak wavelength of 950 nm that was maintained at 1.076 V. As shown in Figure S5A, the ECL spectrum can be fitted to

only one single peak. The ECL spectrum was compared with the PL spectrum of Au_{25}^- shown in Figure 3. The ECL peak wavelength recorded at this potential matches with that (945 nm) of the Au_{25}^- PL (Figure 3A, black curve). The slight red-shift of the ECL spectrum relative to that of PL is related to self-absorption and inner-filter effect due to the higher concentration of ECL relative to PL studies.[1, 28] Also, shown in Figure 3 are the PL spectra of *in-situ* electrogenerated Au_{25}^0 and Au_{25}^+ clusters. These spectra were obtained using an *in-situ* spectroelectrochemical set up (see Experimental), where a 0.1 mM solution of Au_{25}^- (used to obtain the PL in Figure 3A, black) was subjected to preparative electrolysis by applying either a potential of 0.04 V vs. SCE to obtain Au_{25}^0 species (Figure 3A, green curve) or a more positive potential (0.29 V vs. SCE) to further oxidize Au_{25}^0 to Au_{25}^+ (Figure 3A, red curve).

At the onset potential of 0.976 V, Au_{25}^{2+} was generated from Au_{25}^- via sequential oxidation reactions in the vicinity of the electrode (Figure 1). At the same potential the local concentration of TPrA$^\bullet$ concentration (orange solid circle on the cyclic voltammogram in Figure 2B) was much higher than that of Au_{25}^{2+} (recall that TPrA bulk concentration was 125 times higher than Au_{25}^-). The TPaA radical cation generated in eq. 1 might have involved the rduction reactions as well. Thus, the electrogenretated Au_{25}^{2+} was reduced by the TPrA radical (by filling an electron in one of its empty HOMO orbitals), eventually producing Au_{25}^{2-} (eq. 3). The electro- and chemically generated Au_{25}^{2+} and Au_{25}^{2-} can react, generating Au_{25}^{-*} (eq. 4) that returned to the ground state and emitted light at 950 nm (eq. 5). While TPrA$^\bullet$ could react with Au_{25}^{2+} to generate Au_{25}^{+*} by injecting an electron in one of its empty LUMOs, the limited concentration of the reacting species Au_{25}^{2+} near the electrode seemed to undergo several successive reduction reactions with TPrA$^\bullet$ to Au_{25}^{2-}, since no other excited species were observed at the onset potential and the corresponding peak can be just fitted with one peak (*vide infra*). Upon applying a more positive potential, the ECL peak was blue-shifted and its intensity increased. For instance, at 1.276 V, the correlated ECL spectrum showed a peak wavelength of 900 nm, while there was a moderate increase in the ECL intensity (green spectrum in Figure 3B). At this potential the Au_{25}^- was oxidized to Au_{25}^{2+} (eqs. 6-8), which was then reduced to Au_{25}^+ by TPrA$^\bullet$ that is in excess, forming the excited state (Au_{25}^{0*}) (eqs. 9-10). The emission of this excited species is at 900 nm, which is in agreement with the PL peak wavelength (Figure 2, Figure S5B and Figure 3A) (eq. 11) of the *in-situ* formed Au_{25}^0. At this potential the TPrA concentration depletion caused a decrease in the excited state concentration and corresponding emission. The alternative route for Au_{25}^{0*} formation could be electron exchange between Au_{25}^{2+} and Au_{25}^{2-} (eq. 4), which should play a minor role in the emission because of the short lifetime of these two species. The complexity of the proposed mechanisms can be also explored following the simulation techniques.[29]

$$T\,\mathrm{Pr}\,A \rightarrow T\,\mathrm{Pr}\,A^{\bullet+} + e \quad (1)$$

$$T\,\mathrm{Pr}\,A^{\bullet+} \rightarrow T\,\mathrm{Pr}\,A^{\bullet} + H^+ \quad (2)$$

$$Au_{25}^- + T\,\mathrm{Pr}\,A^{\bullet} \rightarrow Au_{25}^{2-} + \mathrm{Pr}_2\,N^+ = CHCH_2CH_3 \quad (3)$$

$$Au_{25}^{2+} + Au_{25}^{2-} \rightarrow Au_{25}^{-*} \quad (4)$$

$$Au_{25}^{-*} \rightarrow Au_{25}^- + hv_1 \quad (5)$$

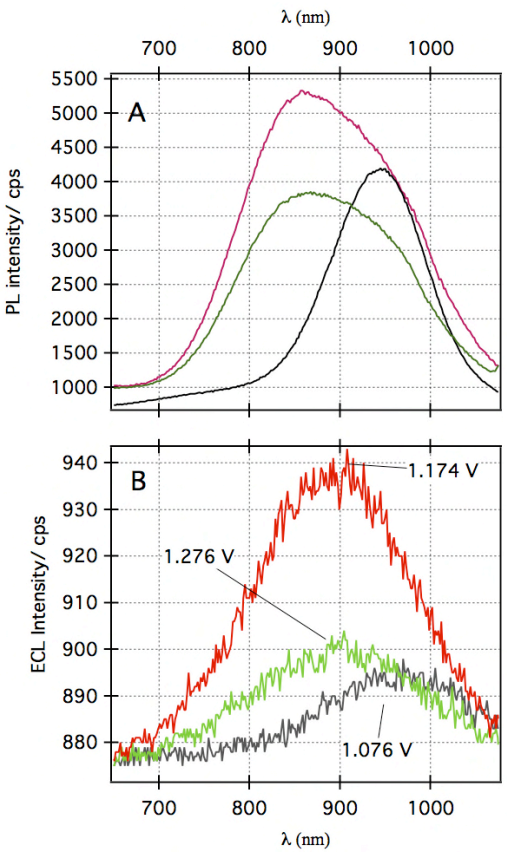

Figure 3. (A) Photoluminescence spectra of Au_{25}^- (black curve), Au_{25}^0 (green curve) and Au_{25}^+ (red curve) in 1:1 acetonitrile: benzene mixture with a concentration of 0.67 mg/mL, which were recorded upon excitation with a 532 nm laser. The Au_{25}^0 and Au_{25}^+ spectra obtained via in-situ electrolysis experiments by applying 0.05 and 0.32 V *vs.* SCE. (B) The matching ECL spectra of Au_{25}^-/ TPrA [12.5 mM] at three applied potentials.

$$Au_{25}^- \rightarrow Au_{25}^0 + e \quad (6)$$

$$Au_{25}^0 \rightarrow Au_{25}^+ + e \quad (7)$$

$$Au_{25}^+ \rightarrow Au_{25}^{2+} + e \quad (8)$$

$$Au_{25}^{2+} + T\,\mathrm{Pr}\,A^{\bullet} \rightarrow Au_{25}^{+} + \mathrm{Pr}_2\,N^+ = CHCH_2CH_3 \quad (9)$$

$$Au_{25}^{+} + T\,\mathrm{Pr}\,A^{\bullet} \rightarrow Au_{25}^{0*} + \mathrm{Pr}_2\,N^+ = CHCH_2CH_3 \quad (10)$$

$$Au_{25}^{0*} \rightarrow Au_{25}^0 + hv \quad (11)$$

Upon reversing the potential scanning direction to cathodic, spooling ECL spectra revealed a significant emission enhancement recorded, with no appreciable change in the ECL peak wavelength relative to that of Au_{25}^{0*} emission. In this potential range, there would be just enough electrogenerated TPrA$^\bullet$ to react with Au_{25}^{2+}. The ET between these two species, resulted in electron injection to the LUMO orbital of the Au_{25}^{2+} forming the Au_{25}^{+*} excited state (eq. 12). This excited species emitted high intensity as shown in the PL experiment (red in Figure 3A) at a similar wavelength to that of Au_{25}^{0*} (900 nm) (eq. 13).

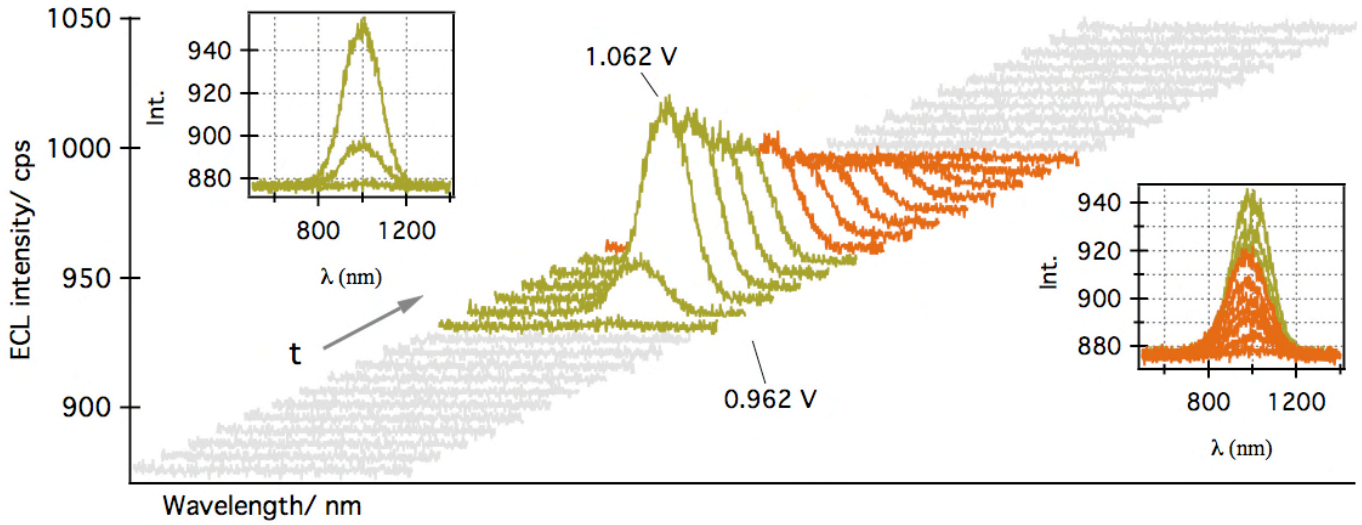

Figure 4. Spooling ECL spectra of 0.1 mM Au_{25}^- in the presence of 200 mM TPrA. Other measuring conditions are the same as in Figure 2. Insets represent stack spectra of ECL evolution (on the left) and devolution (on the right) for clarity of the corresponding peak wavelengths.

$$Au_{25}^{2+} + T\,\mathrm{Pr}\,A^{\bullet} \rightarrow Au_{25}^{+*} + \mathrm{Pr}_2\,N^{+} = CHCH_2CH_3 \quad (12)$$

$$Au_{25}^{+*} \rightarrow Au_{25}^{+} + h\nu \quad (13)$$

$$Au_{25}^{+} + T\,\mathrm{Pr}\,A^{\bullet} \rightarrow Au_{25}^{0} + \mathrm{Pr}_2\,N^{+} = CHCH_2CH_3 \quad (14)$$

$$Au_{25}^{0} + T\,\mathrm{Pr}\,A^{\bullet} \rightarrow Au_{25}^{-} + \mathrm{Pr}_2\,N^{+} = CHCH_2CH_3 \quad (15)$$

To verify the above assessment on the ECL wavelength and intensity pattern, the ECL spectra at 1.076 V, 1.276 V, and 1.174 V (Figure 3B) were plotted along with the PL spectra of the three clusters (Figure 3A). Photoinduced Au_{25}^{-*} (black curve in Figure 3A) emitted at a peak wavelength of 950 nm, which can be distinguished from that of 865 nm (green curve) of the Au_{25}^{0*} and that of 860 nm (purple curve) from the Au_{25}^{+*}. The PL from the Au_{25}^{+*} was more intense than that from the Au_{25}^{0*}. Very interestingly, ECL from the Au_{25}^{-*}, Au_{25}^{0*} and Au_{25}^{+*} were elucidated at the above three applied potentials showed the same changing tendencies in the wavelength and intensity as the PL, which further validate our rational.

The ECL-voltage curve of the above system is shown in Figure S6, where the ECL intensity measured as photocurrent by a photomultiplier tube (PMT) is plotted *vs*. the applied potential. The onset ECL was found to be at 0.876 V, a value in very good agreement with that from the spooling ECL spectroscopy demonstrated above. Less information can be obtained from the ECL-voltage curve than the spooling ECL spectroscopy, because it detects only the total emitted photons. It is noteworthy that in the absence of Au_{25}^- no ECL was observed in a 50 mM TPrA solution (Figure S7) in the same potential window.

The spooling ECL spectra of 0.1 mM of Au_{25}^- solution in the presence of other TPrA concentrations (6.3, 25, 50 and 100 mM) were also examined in a similar way, which are shown in Figures S8-11. Similar results to those with 12.5 mM TPrA were obtained, namely an emission at 950 nm from Au_{25}^{-*} at the onset and then at 900 nm, albeit the ECL intensity varied with the TPrA concentration, following the same mechanisms as those with 12.5 mM TPrA concentration. With higher concentrations, at higher applied potentials the ECL peak clearly shifted to 900 nm, which was assigned to the Au_{25}^{0*} emission based on what we described above (see the stacked ECL spectra in the insets of Figures. S9-S11). At potentials favouring the presence of Au_{25}^{2+} in the vicinity of the working electrode, Au_{25}^{+*} formed (eq.12) and the ECL intensity was enhanced at 900 nm. This shift occurs at 1.076 V for a TPrA concentration of 12.5 mM (Fig. 2), while at 0.976 V for TPrA concentrations of 25 mM (Figure S9) and 50 mM (Figure S10).

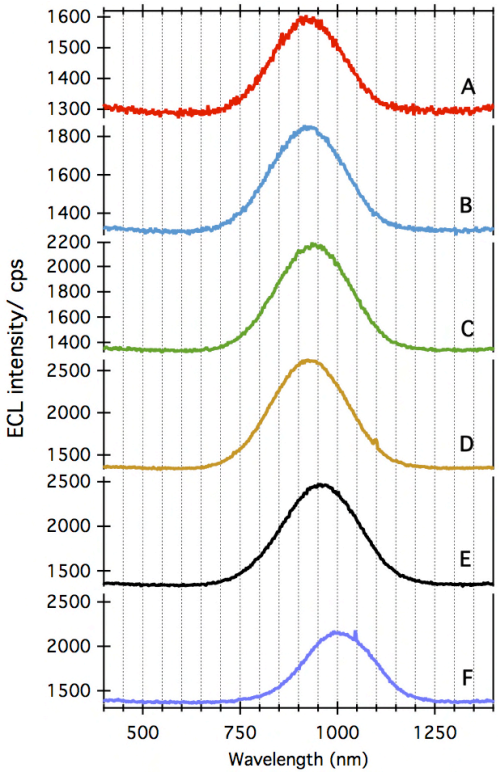

Figure 5. Typical accumulated ECL spectra in the course of potential scanning between -0.324 and 1.324 V *vs*. SCE in the presence of various TPrA concentrations (A-F) with 6.3, 12.5, 25, 50, 100, and 200 mM, respectively. The spectra were obtained within 2 cycles of scanning or 66 s at a scan rate of 100 mVs^{-1}.

With the augmented TPrA concentration, the TPrA$^{\bullet}$ concentration also increases and this favours the reduction reaction of Au_{25}^{+} (eq. 9) to generate the Au_{25}^{0*} (eq. 10). On the other hand, the ECL intensity enhancement appeared constantly at 1.127 V after switching the potential scanning direction, indicating that the formation of Au_{25}^{+*} (eq. 12) was dominant after consuming some TPrA$^{\bullet}$ concentration. Figure S11 shows the spooling ECL spectra of Au_{25}^{-} in the presence of 100 mM TPrA. The left inset of the spectra indicates gradual shift of the ECL peak wavelength to 900 nm during the light evolution, while the right inset of the spectra illustrates sequential peak wavelength shift back to 950 nm.

Due to the high reduction power of the electrogenerated TPrA$^{\bullet}$ species, it can easily act as reducing agent in the bulk solution at higher concentration, and convert the Au_{25}^{-} to Au_{25}^{2-}. With further increased TPrA concentration, to 200 mM for instance, spooling ECL spectra of 0.1 mM Au_{25}^{-} showed a unique peak wavelength at 983 nm, Figure 4. The very high [TPrA$^{\bullet}$] profile with high reducing power kept the Au_{25} oxidation state as the Au_{25}^{2-} (eqs. 9, 14, 15 and 3) in the diffusion layer near the bulk (eq. 3). Au_{25}^{2+} immediately generated in the vicinity of the electrode met and reacted with the Au_{25}^{2-}, favouring the Au_{25}^{-*} generation, eq. 4. This leads to evolution and devolution of ECL at the same wavelength.

The depicted ECL spectrum pattern can be considered as the emission transitions among the three excitation states: ECL is attributed to the Au_{25}^{-*}, Au_{25}^{0*} and Au_{25}^{+*} at low TPrA concentrations and that from the Au_{25}^{-*} is dominant at very high TPrA concentration.

Figure 5 illustrates accumulated ECL spectra recorded during the potential scanning from -0.33 to 1.33 V vs. SCE in two consecutive cycles. There is an interesting trend with the addition of increased TPrA concentration. Basically, there is no pronounced change in peak wavelength with [TPrA] in the concentration range of 6.3 and 50 mM (Figure 5 A-D), with a nominal peak wavelength of 910 nm. The apparent peak wavelength in the presence of 100 mM TPrA (Figure 5E) was shifted to 950 nm, while it was 983 nm with 200 mM [TPrA] (Figure 5F). The trend of the ECL peak shifting is in agreement with the observed features through the spooling experiments described above, moving to a longer wavelength with the increased TPrA concentration from 6.3 to 200 mM. However, spooling ECL spectroscopy provides much more detailed information on ECL mechanisms.

The ECL efficiency was determined as the photons emitted per redox event relative to the $Ru(bpy)_3^{2+}$/TPrA system (Table S1). Due to the depleted PMT sensitivity in the NIR region, the strong ECL might be underestimated. It is plausible that the ECL quantum yields measured by the Andor camera and Acton spectrograph set are more reliable. Please also note that with high [TPrA], the ECL quenching in the $Ru(bpy)_3^{2+}$/TPrA co-reactant system was more dramatic than that in the Au_{25}^{-}/TPrA one.[3] That is the reason why the relative efficiency in Table S1 probably shows overestimated efficiencies with [TPrA] larger than 100 mM. Needless to say, the Au_{25}^{-}/TPrA co-reactant system should have an ECL efficiency > 50% relative to the $Ru(bpy)_3^{2+}$/TPrA.

While the above Au_{25}^{-}/TPrA co-reactant system did produce intermediate ECL intensity, the generation mechanisms showed a zigzagged energy pathway: oxidation of TPrA (eq. 1) and sequential oxidation Au_{25}^{-} to Au_{25}^{2+} (eqs. 6-8) for generating active radicals, and then successive reduction of Au_{25}^{2+} to Au_{25}^{+} by TPrA$^{\bullet}$ (eq. 9) in the vicinity of the electrode and reduction of Au_{25}^{-} to Au_{25}^{2-} (eq. 3) in the bulk for the final generation of the possible three excited states Au_{25}^{-*} (eq. 4), Au_{25}^{0*} (eqs. 10) and Au_{25}^{+*} (eq. 12). While the ECL onset potentials favours the Au_{25}^{-*} generation, the processes to electrogenerate the other two excited states are rather complex, involving many body reactions. Because of the presence of a reduction peak at ~ 1.5 V for Au_{25}^{-}/ Au_{25}^{2-}, it is natural to take considerations of scanning the applied potential in the cathodic region with an electrogenerated oxidative co-reactant such as benzoyl radical (BPO$^{\bullet}$ with E° > +1.5 V *vs*. SCE.[14]). The electrogenerated BPO radical can react with Au_{25}^{2-} to form the Au_{25}^{-*} excited state. In this manner, the zigzagged energy pumping can be avoided.

Electrochemilunnescene of Au_{25}^{-} in the presence of benzoyl peroxide

In the Au_{25}^{-}/ BPO co-reactant system, the reduction of Au_{25}^{-} to Au_{25}^{2-} and the reduction of BPO to produce the oxidizing benzoate radical occurred at very similar potentials, hopefully leading to a more efficient generation of Au_{25}^{-*} than that from the Au_{25}^{+}/BPO co-reactant system we previously published[13]. The electrogenration of Au_{25}^{2-} from the bulk Au_{25}^{-} can happen in smaller potential window rather than reduction of Au_{25}^{+}. Figure 6 shows the ECL-voltage curve (A) and corresponding cyclic voltammogram (CV) (B) of 0.1 mM Au_{25}^{-} with 5 mM BPO. The applied potential was scanned from -0.167 V *vs*. SCE towards more negative values. The onset of ECL-Voltage curve was found to be -0.655 V, at which the BPO reduction (eq. 16) began. The reduction reaction was followed by a decomposition reaction (eq. 17) to the benzoate

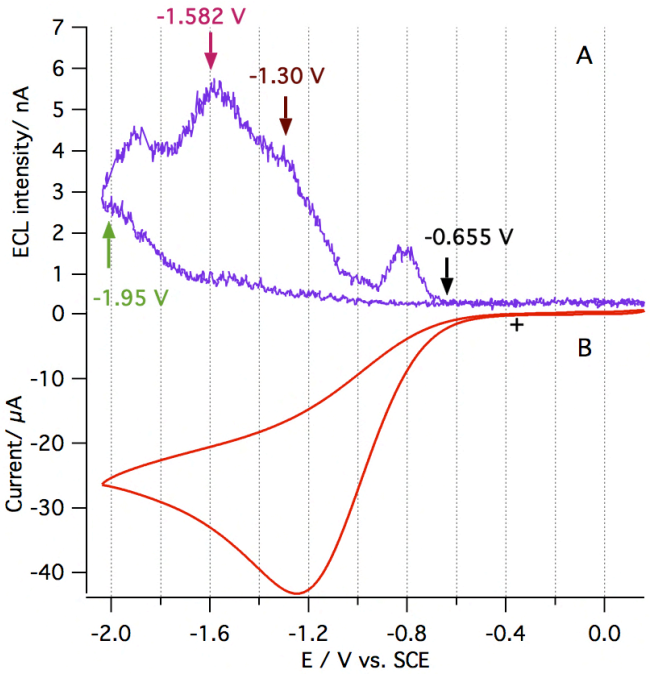

Figure 6. (A) ECL-voltage curve and (B) cyclic voltammogram of 0.1 mM Au_{25}^{-} in the presence of 5 mM benzoyl peroxide (BPO) at a scan rate of 100 mVs^{-1}. The cross indicates starting potential.

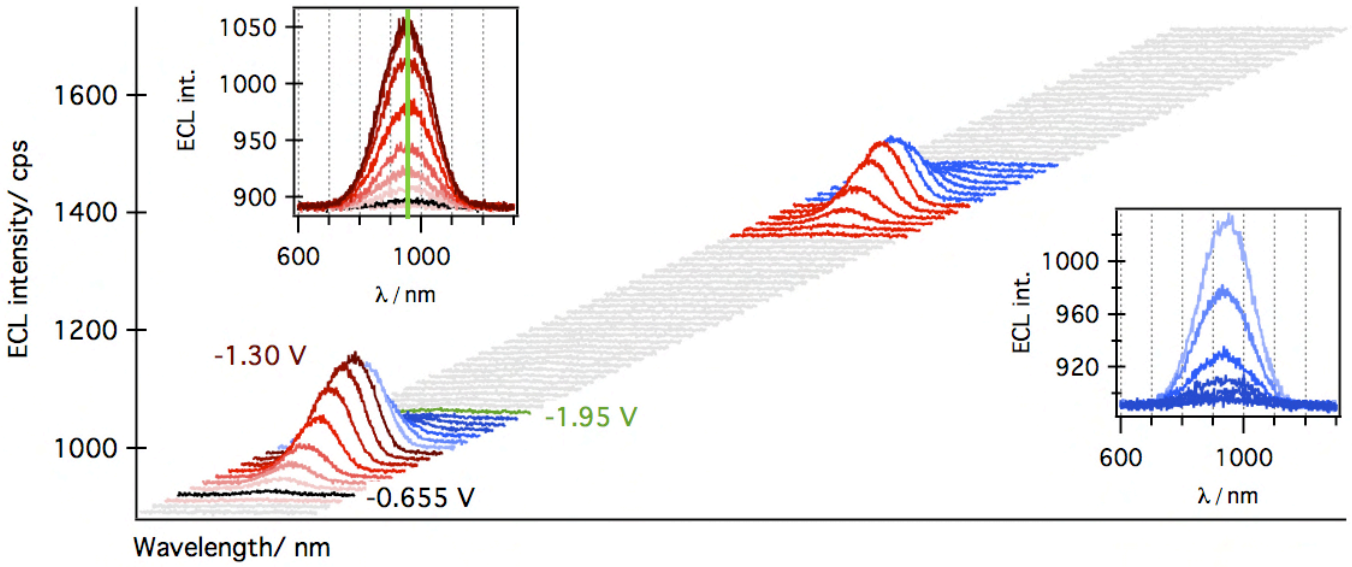

Figure 7. Spooling spectra of 0.1 mM Au_{25}^- in the presence of 5 mM benzoyl peroxide (BPO). The applied Potential was scanned at 100 mVs^{-1} from -0.167 to 1.85 and back to 0.353 V within 83 seconds. Insets are evolution (the red) and devolution (the blue) spectra of the first cycle.

radical ($C_6H_5CO_2^{\bullet}$). The peak at -0.8 V is similar to the previously observed for the Au_{25}^+/BPO co-reactant system, while here is more pronounced due to the different co-reactant concentration, can be generated prior to the reduction of the luminophore.[13] Similar to the Au_{25}^+/BPO co-reactant system,[13] $C_6H_5CO_2^{\bullet}$ accepted one electron from the Au_{25}^- and transformed it to Au_{25}^0 (eq. 18). The Au_{25}^{-*} excited state was generated by transferring one electron from $BPO^{-\bullet}$ to the LUMO of Au_{25}^0 (eq. 18), releasing light upon relaxation to the ground state (eq. 20).

$$BPO + e \rightarrow BPO^{\bullet -} \quad (16)$$

$$BPO^{\bullet -} \rightarrow C_6H_5CO_2^{\bullet} + C_6H_5CO_2^- \quad (17)$$

$$C_6H_5CO_2^{\bullet} + Au_{25}^- \rightarrow Au_{25}^0 + C_6H_5CO_2^- \quad (18)$$

$$Au_{25}^0 + BPO^{\bullet -} \rightarrow Au_{25}^{-*} + BPO \quad (19)$$

$$Au_{25}^- + e \rightarrow Au_{25}^{2-} \quad (20)$$

$$C_6H_5CO_2^{\bullet} + Au_{25}^{2-} \rightarrow Au_{25}^{-*} + C_6H_5CO_2^- \quad (21)$$

Further sweeping the potential to negative values, ECL intensity continued to increase because the reactions showed by eqs. 18-19 were favoured. The ECL intensity reached a maximum at -1.300 V at which potential the benzoate radical formation is at the highest. Continuously moving the potential more negative lead to the reduction of Au_{25}^- to Au_{25}^{2-} (eq. 20 and Figure 1). The Au_{25}^{-*} was generated in this potential region by the reaction of Au_{25}^{2-} with $C_6H_5CO_2^{\bullet}$ in the diffusion layer (eq. 21). The ECL intensity reached the highest at the applied potential of -1.582 V as the result of the balance between the rise of [Au_{25}^{2-}] and depletion of BPO.

NIR ECL light emission in this system occurred at 950 nm upon relaxation of the Au_{25}^{-*} to the ground state (eq. 5), which was confirmed by spooling ECL spectroscopy illustrated in Figure 7.

It is important to note that the Au_{25}^-/ BPO co-reactant system would be more favourable than the corresponding Au_{25}^+/BPO, and higher ECL intensity is anticipated. Figure 7 shows the recorded spooling ECL spectra of the Au_{25}^-/ BPO co-reactant system during two consecutive potential scanning cycles from -0.358 to -2.1 and to 1.62 V. Importantly, the onset ECL spectrum was recorded at -0.655 V, in very good agreement with that of ECL-voltage in Figure 6. As shown in stacked spectra for ECL revolution and devolution, the ECL peak wavelength is constant at 950 nm. This means that the emission is originated from the same Au_{25}^{-*} excited state. The ECL emission of Au_{25}^-/TPrA system reached to 170 count, which is three times higher than the Au_{25}^-/BPO system with the same co-reactant concentration. The BPO concentration was varied from 2.5 to 25 and 50 mM (Figures S12-S14). The lower 2.5 mM concentration did not generate enough of the required BPO radical to observe ECL. In the presence of 25 and 50 mM the intensity of the ECL light emission is low due to the quenching effect of the co-reactant.[30] Thus, the best ECL efficiency with 5 mM BPO was estimated > 30% relative to the $Ru(bpy)_3^{2+}$ system (Table S2 in ESI).

Conclusions

For the first time, ECL of the Au_{25}^- cluster was studied in both annihilation and co-reactant routes. No appreciable ECL was observed in the annihilation path, due to the low reaction rate of the two cluster cores and the short lifetime of the electrogenerated reactive intermediates, the Au_{25}^{2-} and Au_{25}^{2+}. In the presence of TPrA or BPO as the co-reactant, a relatively long-lived strong reducing or oxidizing intermediate was electrogenerated, which can react with various Au_{25} charged species to give off NIR-ECL. The Au_{25}^-/TPrA system showed ECL emissions at 950 and 900 nm. By means of spooling ECL spectroscopy, the two-wavelength ECL was attributed to three excitation states including Au_{25}^{-*}, Au_{25}^{0*} and Au_{25}^{+*}. These were elucidated by comparing the ECL spectra with PL spectra measured with each of the species generated *in-situ*.

Interestingly, the ECL intensity is proportional to the local concentration of these excited states and can be tuned by the applied potential or co-reactant concentration. BPO also enhanced the ECL emission at 950 nm in the NIR region. The study of ECL dependence on the TPrA and BPO concentration revealed that the TPrA system is more efficient than BPO. In the current study, the Au_{25}^{-}/ BPO system is more efficient than our previous Au_{25}^{+}/ BPO system, due to the smaller driving force needed for Au_{25}^{2-} generation. These fundamental studies add to the knowledge of the properties of these interesting small old nanoclusters and the ECL of these nanoclusers is anticipated to have potential applications in electroanalytical sensing and bio-imaging.[31]

Acknowledgements

We are very grateful to the Department of Chemistry, Electronic Shop and ChemBio Store at Western for the great support and quality service. We also thank NSERC for the financial support to this research.

Electronic Supplementary Information (ESI) available: UV-vis-NIR, ^{1}HNMR and ESI mass spectra of Au_{25}^{-}, annihilation ECL-voltage curve of Au_{25}^{-}, curve-fitted spooling ECL spectra, ECL-voltage curves of Au_{25}^{-} with 12.5 and 50 mM TPrA, spooling ECL spectra of Au_{25}^{-} with 6.25, 25, 50 and 100 mM TPrA, ECL-voltage curves, spooling and accumulated ECL spectra of 0.1 mM of Au_{25}^{-} with 5, 25 and 50 mM BPO, PL spectra of Au_{25}^{-} using 633 nm excitation wavelength. See DOI: 10.1039/b000000x/

References:

1. A. J. Bard, *Electrogenerated Chemiluminescence*, Marcel Dekker, 2004.
2. W. Miao, *Chem. Rev.*, 2008, **108**, 2506-2553.
3. R. Y. Lai and A. J. Bard, *J. Phys. Chem. A*, 2003, **107**, 3335-3340.
4. W. Miao, J. Choi and A. Bard, *J. Am. Chem. Soc.*, 2002, **124**, 14478-14485.
5. A. B. Nepomnyashchii, R. J. Ono, D. M. Lyons, C. W. Bielawski, J. L. Sessler and A. J. Bard, *Chemical Science*, 2012, **3**, 2628.
6. W. J. Miao and A. J. Bard, *Anal. Chem.*, 2003, **75**, 5825-5834.
7. N. Sojic, M. Sentic, M. Milutinovic, F. Kanoufi, D. Manojlovic and S. Arbault, *Chemical Science*, 2014, **5**, 2568-2572.
8. F.-R. F. Fan, S. Park, Y. Zhu, R. S. Ruoff and A. J. Bard, *J. Am. Chem. Soc.*, 2009, **131**, 937-+.
9. G.-X. Liang, L.-L. Li, H.-Y. Liu, J.-R. Zhang, C. Burda and J.-J. Zhu, *Chem. Commun.*, 2010, **46**, 2974-2976.
10. R. Hu, W.-C. Law, G. Lin, L. Ye, J. Liu, J. Liu, J. L. Reynolds and K.-T. Yong, *Theranostics*, 2012, **2**, 723-733.
11. L. Li, H. Liu, Y. Shen, J. Zhang and J.-J. Zhu, *Anal. Chem.*, 2011, **83**, 661-665.
12. Y.-M. Fang, J. Song, J. Li, Y.-W. Wang, H.-H. Yang, J.-J. Sun and G.-N. Chen, *Chem. Commun.*, 2011, **47**, 2369.
13. K. N. Swanick, M. Hesari, M. S. Workentin and Z. Ding, *J. Am. Chem. Soc.*, 2012, **134**, 15205-15208.
14. E. A. Chandross and F. I. Sonntag, *J. Am. Chem. Soc.*, 1966, **88**, 1089-1096.
15. Y. Zhu, H. Qian, B. A. Drake and R. Jin, *Angew. Chem. Int. Ed.*, 2010, **49**, 1295-1298.
16. J. F. Parker, J. E. F. Weaver, F. McCallum, C. A. Fields-Zinna and R. W. Murray, *Langmuir*, 2010, **26**, 13650-13654.
17. R. Guterman, M. Hesari, P. J. Ragogna and M. S. Workentin, *Langmuir*, 2013, **29**, 6460-6466.
18. S. Sahami and M. J. Weaver, *J. Electroanal. Chem. and Interfac. Electrochem.*, 1981, **122**, 155-170.
19. D. R. Kauffman, D. Alfonso, C. Matranga, H. Qian and R. Jin, *J. Am. Chem. Soc.*, 2012, **134**, 10237-10243.
20. D. Lee, R. L. Donkers, G. Wang, A. S. Harper and R. W. Murray, *J. Am. Chem. Soc.*, 2004, **126**, 6193-6199.
21. Z. Liu, M. Zhu, X. Meng, G. Xu and R. Jin, *J. Phys. Chem. Lett.*, 2011, **2**, 2104-2109.
22. S. Chen, R. S. Ingram, M. J. Hostetler, J. J. Pietron, R. W. Murray, T. G. Schaaff, J. T. Khoury, M. M. Alvarez and R. L. Whetten, *Science*, 1998, **280**, 2098-2101.
23. M. W. Heaven, A. Dass, P. S. White, K. M. Holt and R. W. Murray, *J. Am. Chem. Soc.*, 2008, **130**, 3754-3755.
24. M. Zhu, C. M. Aikens, F. J. Hollander, G. C. Schatz and R. Jin, *J. Am. Chem. Soc.*, 2008, **130**, 5883-5885.
25. S. A. Miller, C. A. Fields-Zinna, R. W. Murray and A. M. Moran, *J. Phys. Chem. Lett.*, 2010, **1**, 1383-1387.
26. Z. Wu and R. Jin, *Nano Lett.*, 2010, **10**, 2568-2573.
27. S. Antonello, N. V. Perera, M. Ruzzi, J. A. Gascón and F. Maran, *J. Am. Chem. Soc.*, 2013, **135**, 15584-15594.
28. A. B. Nepomnyashchii, M. Broering, J. Ahrens, R. Krueger and A. J. Bard, *J. Phys. Chem. C*, 2010, **114**, 14453-14460.
29. O. V. Klymenko, I. Svir and C. Amatore, *Chem. Phys. Chem.*, 2013, **14**, 2237-2250.
30. J.-P. Choi, Ph.D Dissertation, The University of Texas at Austin, 2003.
31. V. W. K. Ng, R. Berti, F. Lesage and A. Kakkar, *J. Mater. Chem. B*, 2013, **1**, 9-25.

Table of Content:

By means of spooling spectroscopy, we demonstrate our discovery on near-infrared electrochemiluminescence of Au_{25}^- nanoclusters at 950 and 900 nm, which can be attributed to the Au_{25}^{-*}, Au_{25}^{0*} and Au_{25}^{+*} excited species being controllable chemically and electrochemically.